

See discussions, stats, and author profiles for this publication at: <https://www.researchgate.net/publication/277603059>

Matrix Stiffness and Nanoscale Spatial Organization of Cell-Adhesive Ligands Direct Stem Cell Fate

ARTICLE *in* NANO LETTERS · JUNE 2015

Impact Factor: 13.59 · DOI: 10.1021/acs.nanolett.5b01619 · Source: PubMed

CITATIONS

4

READS

59

7 AUTHORS, INCLUDING:



Kai Ye

Fudan University

7 PUBLICATIONS 60 CITATIONS

[SEE PROFILE](#)



Xuan Wang

Fudan University

7 PUBLICATIONS 74 CITATIONS

[SEE PROFILE](#)



Shiyu Li

Fudan University

5 PUBLICATIONS 15 CITATIONS

[SEE PROFILE](#)

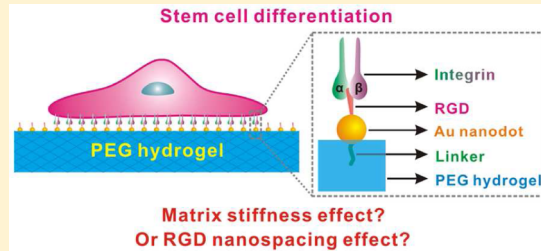
Matrix Stiffness and Nanoscale Spatial Organization of Cell-Adhesive Ligands Direct Stem Cell Fate

Kai Ye, Xuan Wang, Luping Cao, Shiyu Li, Zhenhua Li, Lin Yu, and Jiandong Ding*

State Key Laboratory of Molecular Engineering of Polymers, Collaborative Innovation Center of Polymers and Polymer Composite Materials, Department of Macromolecular Science, Advanced Materials Laboratory, Fudan University, Shanghai 200433, China

ABSTRACT: One of the breakthroughs in biomaterials and regenerative medicine in the latest decade is the finding that matrix stiffness affords a crucial physical cue of stem cell differentiation. This statement was recently challenged by another understanding that protein tethering on material surfaces instead of matrix stiffness was the essential cue to regulate stem cells. Herein, we employed nonfouling poly(ethylene glycol) (PEG) hydrogels as the matrix to prevent nonspecific protein adsorption, and meanwhile covalently bound cell-adhesive arginine-glycine-aspartate (RGD) peptides onto the hydrogel surfaces in the form of well-defined nanoarrays to control specific cell adhesion. This approach enables the decoupling of the effects of matrix stiffness and surface chemistry. Mesenchymal stem cells (MSCs) were cultured on four substrates (two compressive moduli of the PEG hydrogels multiplied by two RGD nanospacings) and incubated in the mixed osteogenic and adipogenic medium. The results illustrate unambiguously that matrix stiffness is a potent regulator of stem cell differentiation. Moreover, we reveal that RGD nanospacing affects spreading area and differentiation of rat MSCs, regardless of the hydrogel stiffness. Therefore, both matrix stiffness and nanoscale spatial organization of cell-adhesive ligands direct stem cell fate.

KEYWORDS: Matrix stiffness, stem cell differentiation, nanopattern, RGD nanospacing, poly(ethylene glycol) (PEG) hydrogel, cell adhesion



Stem cells reside in a niche that is composed of neighboring cells, extracellular matrix (ECM), autocrine and paracrine soluble growth factors, and so forth.¹ The interplay between stem cells and these components appears to be rather intricate, among which stem cell-ECM interactions receive particular concerns.^{2,3} During the past decade, cell-material interactions has been an emerging research front in the fields of biomaterials and regenerative medicine.^{4–6} Material scientists have been attempting to design a variety of biomimetic materials to simulate the interactions between cells and ECM.^{4,7,8} Cell behaviors are influenced by chemical cues,⁹ such as chemical composition,¹⁰ molecular chirality,¹¹ and ligand density,¹² as well as physical cues,¹³ such as matrix stiffness,^{14,15} surface topography,¹⁶ and interfacial hydrophobicity,¹⁷ of the micro-environment. Matrix stiffness, an inherent mechanical property of ECM, has a profound impact on adhesion,^{18–20} migration,^{21,22} proliferation,²³ and differentiation²⁴ of anchorage-dependent cells. Stem cells show lineage-specific commitments when cultured on substrates matching the stiffnesses of the corresponding tissues *in vivo*.^{25,26} Soft substrates are beneficial for a neurogenic or adipogenic differentiation, stiff substrates are beneficial for an osteogenic differentiation, and substrates of an intermediate stiffness favor a myogenic lineage commitment, for “tissue cells feel and respond to the stiffness of their substrate” as indicated by Discher et al.^{14,25}

However, a controversy upon this famous viewpoint was launched recently. On the basis of a series of elegant experiments, Watt and Huck groups argued that stiffness

could not be the real reason itself but influenced stem cell differentiation indirectly by varying surface chemistry such as protein tethering, for “cell spreading and differentiation were unaffected by polydimethylsiloxane stiffness”, and polyacrylamide “hydrogels of different stiffnesses will lead to differences in anchoring densities and thereby alter the mechanical feedback of the collagen”.²⁷ Soon after, Engler group defended their stiffness effect and indicated that “differentiation does not depend on tethering”.²⁸ Which is the essential cue to influence stem cell differentiation, matrix stiffness or surface chemistry? It constitutes one of the critical fundamental questions for biomaterials and regenerative medicine.

Although the responses of stem cells to matrix stiffness have been widely investigated, little research fully eliminated other interferential factors, especially protein adsorption onto the matrix surfaces in culture medium with serum. To decouple the stiffness effect from surface chemistry effect, a surface patterning technique was employed in the present study. Nanopatterns of arginine-glycine-aspartate (RGD), an oligopeptide sequence existing in some ECM proteins, enable precise control of cell adhesion sites.²⁹ Specific cell adhesion is formed via the bioconjugation of RGDs and the transmembrane receptors integrins, followed by the activation of

Received: April 24, 2015

Revised: May 10, 2015

the downstream focal adhesion (FA) complexes.^{30,31} Considering that the size of an integrin is 8–12 nm,³² it is of great value to generate RGD nanopatterns with RGD binding sites of approximately 10 nm, which can be achieved by block copolymer micelle nanolithography.^{33,34} Thus, integrin distribution could be controlled by RGD organization on the molecular level. To date, quite a lot of investigations have been made on the preparation of RGD nanoarrays,^{35–38} microislands,^{39–41} or microislands of nanoarrays.^{42–44} A critical RGD nanospacing of 70 nm has been proposed, beyond which a sharp decrease of cell adhesion was observed.^{45,46} A well-controlled surface chemistry via RGD nanopatterning affords a basis for a deterministic examination of the effect of matrix stiffness.

A prerequisite for the study of cell adhesion and subsequent cell differentiation on RGD nanopatterns is to ensure that the background material possesses strong and persistent resistance to protein adsorption and cell adhesion for several days. Poly(ethylene glycol) (PEG) is a powerful nonfouling molecule, and in this study a PEG hydrogel is selected as the nonfouling background due to its better performance than a self-assembled monolayer.⁴⁷ Another motivation for us to choose the PEG hydrogel comes from the tunability of its stiffness.⁴⁸ Hence, an RGD-nanopatterned PEG hydrogel serves as a perfect platform for the study of matrix stiffness effect on stem cell differentiation.

Herein, we examined the effect of matrix stiffness on stem cell behaviors in a well-controlled surface chemistry, as schematically depicted in Figure 1. RGD nanopatterns on

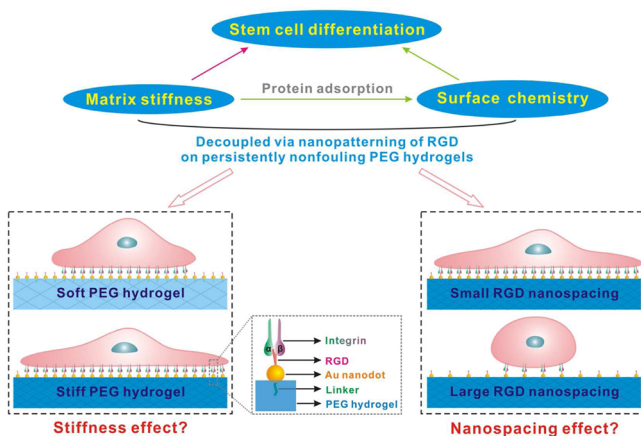


Figure 1. Schematic illustration of the idea to investigate the effects of stiffness of matrix and organization of cell-adhesive ligands on adhesion and differentiation of stem cells. Mesenchymal stem cells were seeded on RGD nanopatterns of varied nanospacings on nonfouling PEG hydrogels of different stiffnesses. Cells underwent osteogenic and adipogenic coinduction after initial adhesion. The stiffness effect was examined at a given RGD nanospacing, and the nanospacing effect was studied at a given hydrogel stiffness.

nonfouling PEG hydrogels were generated, with RGD nanospacings of 49 and 135 nm. Mesenchymal stem cells (MSCs) derived from bone marrows of rats were induced in the mixed osteogenic and adipogenic medium for 7 days after 1 day of initial adhesion. Our study was carried out by varying hydrogel stiffness or RGD nanospacing independently, which enabled the determination of the stiffness effect and the nanospacing effect in a decoupled way.

The stiffness control of PEG hydrogels could be realized by changing the molecular weight of poly(ethylene glycol)-diacrylate (PEG-DA) macromer and varying the concentration of PEG-DA in its aqueous solution. An increase of the chain length of PEG-DA resulted in softening of the hydrogel after polymerization of the macromers; an increase of the macromer concentration led to hardening of the hydrogel. PEG-DA macromers with four different molecular weights were acquired. PEG-700-DA was purchased from Sigma-Aldrich, and the other three PEG-DA macromers were self-synthesized by the reaction of PEGs and acryloyl chloride (Figure 2a).

Photopolymerization of PEG-DA macromers was carried out to form PEG hydrogels (Figure 2a). PEG-DAs with number-average molecular weights M_n 4k, 10k, and 20k were dissolved in Milli-Q water to achieve a range of concentrations from 16.7 to 50.0% (w/w), and PEG-700-DA was directly used or diluted with Milli-Q water to a range of concentrations from 20.0 to 100% (w/w). Polymerization was initiated by 2-hydroxy-4'-(2-hydroxyethoxy)-2-methylpropiophenone (D2959, Aldrich) with weight fraction over macromer 0.05% (w/w) under ultraviolet radiation (365 nm). The stiffness of the hydrogel was quantified by compressive modulus, which was read from the slope of the stress-strain curve at low strains ($\leq 5\%$) measured in a rheometer (Kinexus Pro, Malvern, U.K.). A set of stress-strain data is demonstrated in Figure 2b. The moduli were tuned over 3 orders of magnitude, ranging from 8 kPa to 3.2 MPa (Figure 2c), covering the majority of the stiffness range of living organisms.

We fabricated RGD nanopatterns on PEG hydrogels using a transfer strategy, as schematically presented in Figure 3. Because of the difficulty to directly generate a stable RGD nanoarray on a polymeric substrate, we first prepared nanopatterns on glass via block copolymer micelle nanolithography (Figure 3a) and then transferred the patterns to PEG hydrogels (Figure 3b). Block copolymers of poly(styrene-block-2-vinylpyridine) (PS-*b*-P2VP, Polymer Source) were used as polymeric templates. The copolymers formed reversed micelles in toluene with poly(2-vinylpyridine) blocks as cores and polystyrene blocks as coronae. A metal precursor hydrogen tetrachloroaurate(III) hydrate ($\text{HAuCl}_4 \cdot 3\text{H}_2\text{O}$, Alfa Aesar) was loaded into the hydrophilic P2VP cores. A self-assembled monolayer of the micelle solution was dip-coated onto a glass surface. Afterward, the block copolymer template was removed by oxygen plasma treatments, and the gold precursor was reduced to gold after further exposure in the air, resulting in a hexagonal gold nanoarray on glass.

The micelle patterns were demonstrated by observations in a transmission electron microscope (TEM, Tecnai G2 20 TWIN, U.S.A.), as shown in Figure 4a. Gold nanopatterns were characterized in an atomic force microscope (AFM, Multimode 8, Bruker, U.S.A.). The gold nanodots possessed sizes of approximately 10 nm (Figure 4b), which matched the size of an integrin, the transmembrane receptor of RGD. The interparticle spacing of the gold nanodots was controlled by varying the block length or the concentration of the block copolymer. Longer block lengths or lower concentrations led to larger intervals between closely packed micelles. Gold patterns of two nanospacings were fabricated on glass, as observed in a field-emission scanning electron microscope (FE-SEM, Ultra 55, Zeiss, Germany) (Figure 4c, top row), and the average nanospacings were calculated using the software ImageJ (freely available at <http://www.nih.gov>). The parameters of the prepared Au nanopatterns are listed in Table 1.

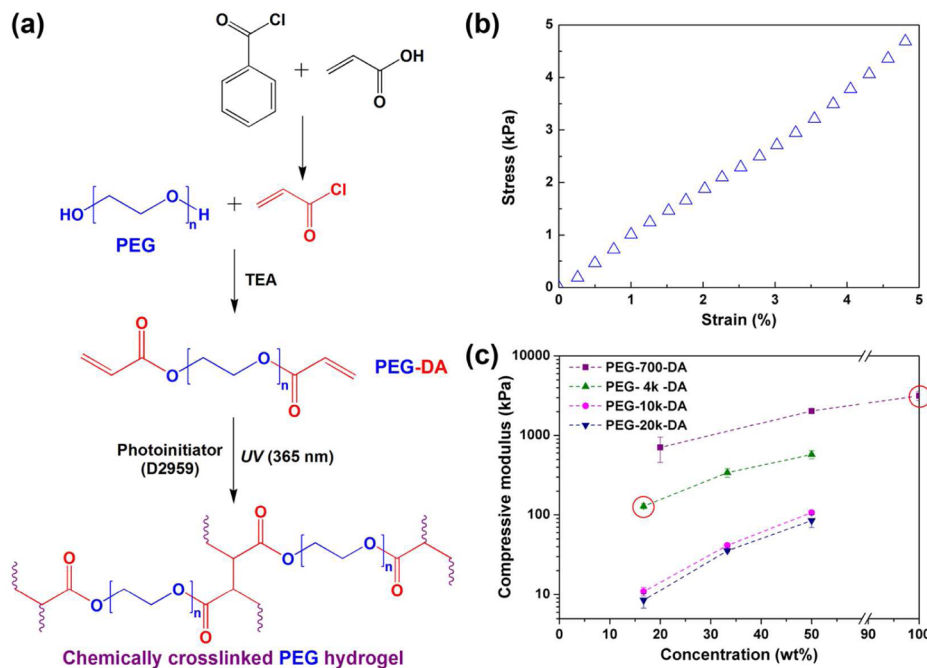


Figure 2. Synthesis routes of PEG-DA macromers and PEG hydrogels and mechanical characterization of the resultant hydrogels. (a) Preparation of PEG hydrogels. PEG-DAs were synthesized via the reaction of fresh distilled acryloyl chloride and PEGs using triethylamine (TEA) as the proton scavenger, and PEG hydrogels were formed via photopolymerization of PEG-DAs. (b) Demonstrated stress–strain data collected in a rheometer. A linear fitting at low strains ($\leq 5\%$) led to compressive modulus. (c) The compressive moduli of PEG hydrogels after swelling in phosphate buffer saline (PBS) at 37°C . The hydrogels were obtained by chemical cross-linking of the indicated macromers. The red circles mark the two cases used in the later experiments.

To study the stiffness effect on cell behaviors on nano-patterned surfaces, gold nanopatterns were transferred to nonfouling PEG hydrogels of different stiffnesses using a unique transfer lithography technique.⁴⁹ Very soft hydrogels were not recommended for subsequent cell studies due to the difficulty of a complete transfer of nanopatterns from glass to hydrogels. Samples of Au nanopatterns were immersed in the linker solution to graft with a heterobifunctional linker *N,N'*-bis(acryloyl) cystamine (Sigma). Next, a mixture of PEG-DA macromer and photoinitiator D2959 was added onto the glass, and photopolymerization was initiated by ultraviolet radiation under the protection of nitrogen atmosphere. The thiol groups of the linkers formed covalent bonds with Au nanodots, and the double bonds participated in PEG-DA polymerization to constitute the cross-linked network. The successful transfer of gold nanopatterns to PEG hydrogels was confirmed by FE-SEM images, as presented in the middle and the bottom rows of Figure 4c.

It seems worthy of noting that the densities of the gold nanodots on the PEG-4k hydrogels in Figure 4c are higher than those on the corresponding PEG-700 hydrogels or on glass surfaces, simply due to dehydration of the former prior to the SEM observation. The as-polymerized PEG-700 gels were free of water, because PEG-700-DA macromers were liquid and available to be polymerized directly; in contrast, the as-polymerized PEG-4k hydrogels contained much water because PEG-4k-DA macromers were solid and needed to be dissolved in water before polymerization. Unless observed in cryo-SEM, the nanospacings on the dehydrated PEG-4k hydrogels in FE-SEM images must be significantly smaller than those on the corresponding PEG-700 hydrogels or on glass surfaces. In the later experiments for cell studies, RGD nanospacing was

determined via the spacing on glass multiplied by the linear swelling ratio of the as-polymerized hydrogel in PBS at 37°C .

The different chain lengths and concentrations of the macromers in Figure 2c influenced not only the stiffnesses but also the swelling ratios of the hydrogels in an aqueous environment. The different swelling ratios might bring us much difficulty to maintain a constant RGD nanospacing in the examination of the stiffness effect on cell adhesion and differentiation. After a careful pretry, we selected the two hydrogels as indicated in Table 2 to guarantee the same swelling ratio in PBS at 37°C . Thus, transferring a nanopattern on glass prepared via one block copolymer template onto these two hydrogels resulted in the same nanospacing even after swelling of the PEG hydrogels in an aqueous environment. As summarized in Table 1, the eventual nanospacings were 49 and 135 nm for the copolymers of two different block lengths, irrespective of the hydrogels obtained from two different macromer lengths and concentrations.

The compressive moduli of the hydrogels examined in the forthcoming cell experiments were 130 and 3170 kPa, respectively, as listed in Table 2. These two hydrogels are denoted as relatively “soft” and “stiff” ones in this study. Here, linear swelling ratio was measured from the ratio between the diameters of a circular hydrogel sheet after and before swelling in the indicated aqueous environment. In order to determine gel content, an as-prepared hydrogel was dried first and weighed as W_0 . Then the residual unreacted macromers in the gel were extracted thoroughly by dichloromethane (DCM) for 72 h, and the redried gel was weighed as W . The ratio between W and W_0 gave gel content. It is a measure of the cross-linking extent in the hydrogel: a higher gel content indicates that more macromers were cross-linked into the gel network. The gel contents of the two hydrogels were both above 90%,

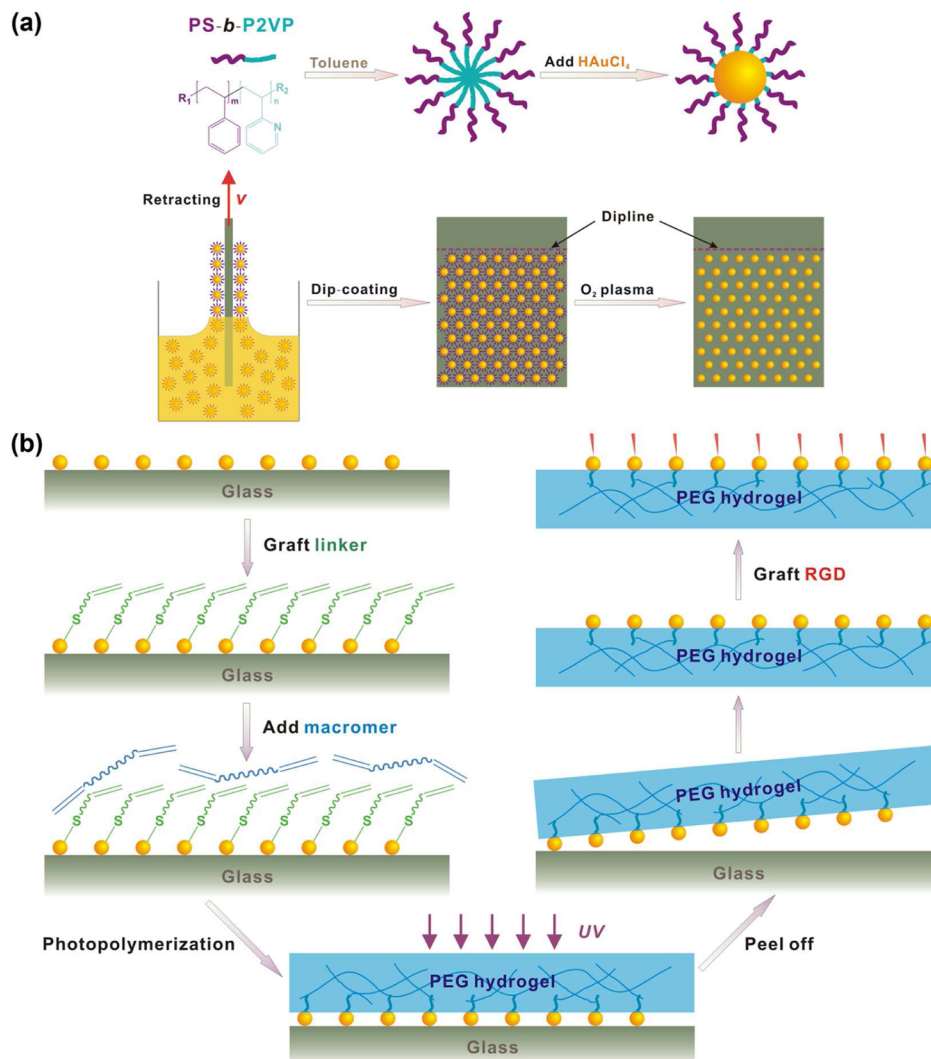


Figure 3. Schematic presentation of fabrication procedures of RGD nanopatterns on nonfouling PEG hydrogels. (a) Preparation of Au nanopattern on glass via block copolymer micelle nanolithography. Dip-coating was conducted to generate an array of micelles with the cores loaded with a gold precursor, and the gold nanopattern on glass was obtained after plasma treatments to remove the polymer and reduce the gold precursor. (b) Preparation of an RGD-nanopatterned PEG hydrogel via transfer lithography. The gold nanodots on glass were grafted with the linkers and transferred to a PEG surface upon photopolymerization of PEG-DA. RGD peptides were grafted onto the gold nanodots to achieve cell-adhesive motifs.

confirming considerable polymerization extents of the macromers in our experiments.

Prior to cell seeding, gold nanopatterns were grafted with cell-adhesive peptides by soaking PEG hydrogels in 25 μ M aqueous solution of c(-RGDfK)-thiol (f: d-phenylalanine, K: L-lysine; Peptides International). Such a cyclic RGD was initially designed by Kessler⁵⁰ and has been widely applied in biomaterials and cell studies.^{51–53} After the cyclic RGD peptides were bound to the gold nanoparticles via the S-Au covalent bonds, RGD nanopatterns on PEG hydrogels were eventually achieved with RGDs as the nanoscale cell-adhesive sites and PEG hydrogels as the anticell-adhesive background.

MSCs derived from tibias and femurs of neonatal Sprague-Dawley (SD) rats were employed as the model cells. MSCs of the second passage were used for adhesion and subsequent differentiation assays. To evaluate the effects of hydrogel stiffness and RGD nanospacing on cell adhesion, we seeded stem cells on sterilized nanopatterned surfaces at a density of 6500 cells per cm^2 . Cells were allowed to adhere onto RGD

nano-patterns in the growth medium, which was composed of low-glucose Dulbecco's modified Eagle medium (DMEM, Gibco) supplemented with 10% fetal bovine serum (FBS, Gibco), 100 U/mL penicillin (Gibco), 100 μ g/mL streptomycin (Gibco) and 2 mM L-glutamine (Gibco), for 24 h. Immunofluorescent staining was carried out for visualization of vinculins (green), filamentous actins (F-actins, red) and nuclei (blue). Microscopic observations of the fluorescently stained cells were conducted in an inverted microscope (Axiovert 200, Zeiss, Germany) mounted with a color charge coupled device (CCD, AxioCam HRC, Zeiss, Germany). Cell nuclei were counted to obtain cell density. Single cells were outlined using ImageJ software to measure cell spreading areas and determine the fluorescent intensities of F-actins. Three independent experiments were carried out for each group, and more than 200 single cells in each experiment joined in statistical analysis.

Typical fluorescence images are shown in Figure 5a. F-actin is a crucial component of the cytoskeletons, and vinculin is a key protein in FA plaques that is involved in the linkage of

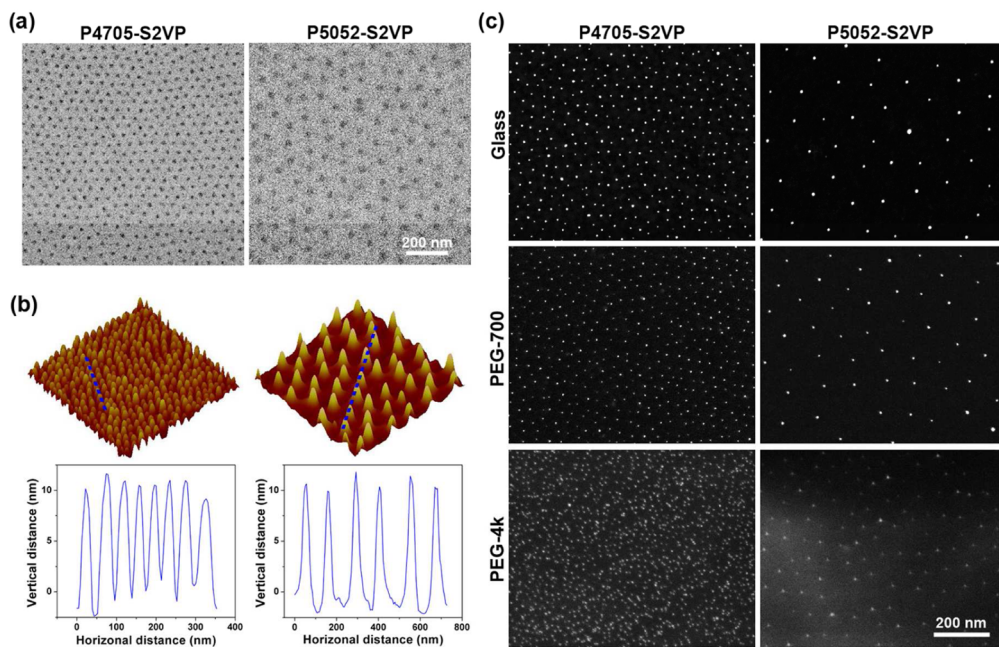


Figure 4. Morphological observations of nanopatterns. (a) TEM images of micelles of the indicated block copolymers after loaded with chloroauric acid into the lipophobic P2VP cores. (b) AFM images of Au nanopatterns of two nanospacings on glass. The upper and the lower rows show AFM images and the height profiles of the sections along the dashed lines, respectively. The area of each image is 750 nm × 750 nm. The diameters of the gold nanodots were about 10 nm according to the heights in the line charts. (c) FE-SEM images of Au nanopatterns of two nanospacings on glass surfaces and on PEG hydrogels of different stiffnesses before swelling. All of the images were captured at dry states. The as-synthesized PEG-700 gels contained no water. The water-containing PEG-4k hydrogels were dehydrated step by step in ethanol, prior to the SEM observation.

Table 1. Fabrication Parameters and Corresponding Nanospacings of Au Nanopatterns Used in This Study

block copolymer	M_n	ratio of S to 2VP units	c^a (mg/mL)	LA ^b	v^c ($\mu\text{m}/\text{s}$)	nanospacing before swelling ^d (nm)	mean nanospacing after swelling ^e (nm)
P4705-S2VP	42500	288:119	7.1	0.64	400	43 ± 1	49
P5052-S2VP	217000	1776:304	3.0	0.44	210	117 ± 6	135

^aConcentration of the block copolymer PS-P2VP in toluene. ^bLoading amount of HAuCl₄ in the block copolymer. ^cRetracting velocity in dip-coating. ^dLateral spacing of Au nanodots on glass or on PEG hydrogels before swelling. ^eAverage lateral spacing of Au nanodots or RGD peptides on PEG hydrogels after swelling in PBS at 37 °C. The swelling ratios of PEG-4k (16.7 wt %) and PEG-700 (100 wt %) in PBS at 37 °C were both 1.15.

Table 2. Parameters of PEG Hydrogels Used for the Transfer of Au Nanopatterns and Subsequent Cell Studies

PEG hydrogel	c^a (w/w)	GC ^b	$LSR_{W, 25^\circ\text{C}}^c$	$LSR_{P, 37^\circ\text{C}}^d$	compressive modulus ^e (kPa)
PEG-4k	16.7%	(92.0 ± 0.5) %	1.21 ± 0.01	1.15 ± 0.01	130 ± 10
PEG-700	100%	(98.8 ± 0.6) %	1.15 ± 0.01	1.15 ± 0.01	3170 ± 413

^aConcentration of PEG-DA macromer in the water solution. ^bGel content. ^cLinear swelling ratio in Milli-Q water at 25 °C. ^dLinear swelling ratio in PBS at 37 °C. ^eCompressive modulus after swelling in PBS at 37 °C.

integrins to the actin cytoskeletons.⁵⁴ Mature focal adhesions were observed to be densely distributed in clusters around the periphery of cells on RGD nanopatterns of the small nanospacing, especially on the stiff hydrogels (Figure 5a, lower row). On patterns of the large nanospacing, immature focal adhesions were vague and distributed in a diffuse manner. Similarly, clear microfilaments and well-organized actin assembly occurred on RGD nanopatterns of the small nanospacing. Compared to the soft hydrogels, stronger focal adhesions and clearer stress fibers were observed on the stiff ones with the small RGD nanospacing.

Statistical results of cell adhesion are shown in Figure 5b–e. With the increase of RGD nanospacing, both cell density (Figure 5b) and spreading area (Figure 5c) declined, regardless of the stiffness of PEG hydrogels, which was consistent with the

previous reports of cell adhesion on glass or PEG-700 hydrogels.^{37,46}

The present study further illustrated the different RGD nanospacing dependences between the soft and the stiff hydrogels. We define the decrease of a cell parameter Q with RGD nanospacing at a given matrix stiffness as

$$\text{Decline rate} = \frac{Q_{\text{small}} - Q_{\text{large}}}{Q_{\text{small}}} \times 100\% \quad (1)$$

Here, Q_{small} and Q_{large} refer to the parameters of cells on nanopatterns of the small and the large RGD nanospacings, respectively.

As shown in Figure 5e, the stiff hydrogels exhibited a more significant nanospacing effect. Platzman et al. suggested that the nanoscale topographies on the surfaces of the soft hydrogels might contribute to the promotion of cell adhesion, especially

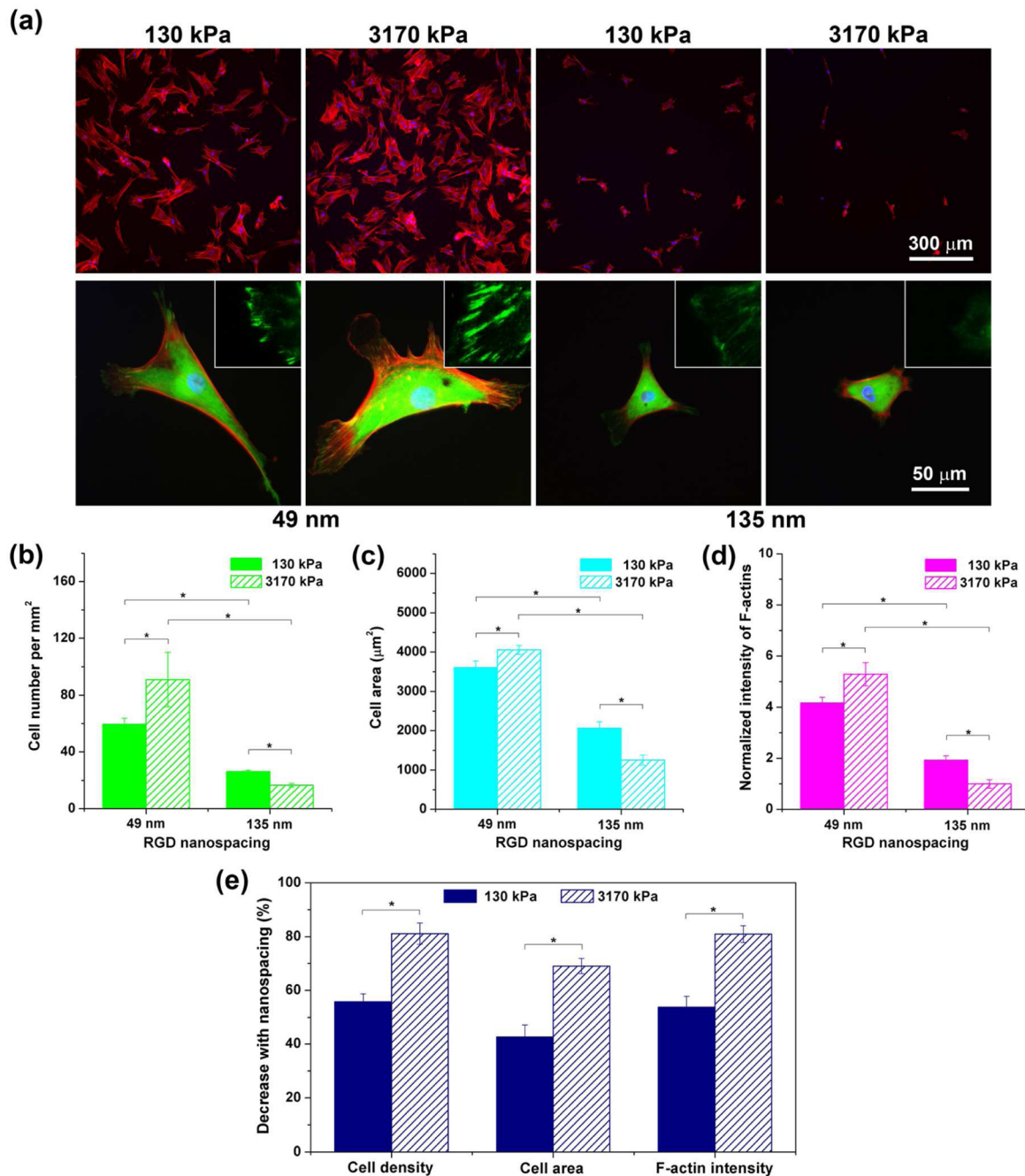


Figure 5. Fluorescence images of cells on RGD-nanopatterned PEG hydrogels and corresponding statistical results as functions of hydrogel stiffness and RGD nanospacing. (a) Cells were cultured on RGD nanopatterns for 24 h and stained for observations of vinculins (green), F-actins (red), and nuclei (blue). The upper and the lower rows show typical low-magnification and high-magnification fluorescence micrographs, respectively. The insets in the lower row demonstrate further magnified local images to show vinculins around the periphery of cells. (b–d) Statistical results of cell density (b), cell spreading area (c), and fluorescent intensity of F-actins normalized to the mean value of the group of the stiff hydrogels (3170 kPa) with the large RGD nanospacing (135 nm) (d). Mean values and standard deviations from three independent experiments are presented. (e) Dependence of the indicated parameters upon RGD nanospacing as characterized by the decline percentage at a given matrix stiffness calculated with eq 1 ($n = 3 \times 3$). “*”: $p < 0.05$ in a student’s *t*-test, indicating a significant difference between the two groups.

on patterns of a large nanospacing, because specific cell adhesion was weak on nanopatterns of spacings beyond the critical nanospacing of around 70 nm.⁵⁵ On our patterns of the small RGD nanospacing, cells were able to form stable specific adhesion, and thus the stiffness effect was predominant over the surface topography effect. Therefore, it is the data from the small RGD nanospacing on the PEG hydrogels that can better reflect the stiffness effect on cell behaviors.

We further made semiquantitative analysis of fluorescent intensity of F-actins of single cells, which illustrated the strength of cell tension to a certain extent (Figure 5d). The average fluorescent intensity of F-actins of cells on the stiff hydrogels with the large RGD nanospacing was set as 1, to which the fluorescent intensities of F-actins in other groups were normalized. The variation tendency of normalized intensity of F-actins was similar to that of cell density or

spreading area. With the increase of RGD nanospacing, F-actin intensity was weakened on both the soft and the stiff hydrogels. On patterns of the small nanospacing, F-actin intensity was higher on the stiff hydrogels, indicating stronger cell tension.

Whereas possible nonspecific cell adhesion on the soft hydrogels increases the complexity of the results on patterns of the large nanospacing, statistical results of cells on RGD nanopatterns of the small nanospacing unambiguously reflect the effect of matrix stiffness. Under this circumstance, cells adhered and spread better, and generated more cell tension on the stiff hydrogels, consistent with the previous publication on unpatterned polyacrylamide gels.¹⁸ Moreover, our results demonstrate that both hydrogel stiffness and RGD nanospacing influence cell adhesion.

For investigation of the effects of matrix stiffness and RGD nanospacing on lineage commitments of stem cells, we incubated MSCs in the mixed osteogenic and adipogenic medium for 7 days following 1 day of adhesion. The medium was a 1:1 mixture of the osteogenic induction medium and the adipogenic induction/maintenance medium.⁵⁶ The mixed medium was replaced every 2–3 days, and 0.5 µg/mL Aphidicolin (Sigma) was added from the fourth to the fifth day to inhibit cell proliferation. After 7 days of coinduction, cells were conducted with alkaline phosphatase (ALP) and oil-droplet staining. ALP was stained first with Fast Blue RR (Sigma), followed by the staining of oil droplets with Oil Red O (Sigma-Aldrich). Cell nuclei were counterstained with 4',6-diamidino-2-phenylindole (DAPI, Sigma-Aldrich) to enable the counting of cell numbers. Four independent experiments were carried out for each group.

It is very challenging for a material to keep nonfouling in such a long period with 1 day of cell adhesion and 7 days of induction with 10% serum. Therefore, we checked the long-term antiadhesion properties of the PEG hydrogels first. The dipline, which emerged as the boundary between the nanopatterned and the unpatterned regions in dip-coating, facilitated our verification. After 1 day of adhesion, stem cells could only be observed in the patterned areas, as shown in the left picture of Figure 6. Even after 8 days of culture and coinduction, the dipline was still very clear, and cells were strictly confined in the patterned regions and could scarcely be seen on the PEG background (Figure 6, right picture). Such an evident contrast of cell adhesion confirmed the strong and persistent resistance of PEG hydrogels to nonspecific cell adhesion and convinced our later differentiation results from the examination of the stiffness effect by ruling out the interference of protein adsorption.

Representative micrographs of cells after coinduction are presented in Figure 7. Cells with blue staining of ALP by Fast Blue RR indicated those osteogenically differentiated, and cells with red fat vacuoles indicated those adipogenically differentiated. Cells with neither successful ALP staining nor oil droplets were undifferentiated. Osteogenesis extent was indicated by the percentage of ALP positive cells (Figure 8), which was calculated by the number of ALP positive cells divided by the number of total cells. Adipogenesis extent was conveyed by the percentage of oil-droplet positive cells. Higher percentage of ALP positive cells indicated better osteogenesis, while higher percentage of oil-droplet positive cells indicated better adipogenesis. Hydrogel stiffness exerted a significant effect on lineage commitments of stem cells. When RGD nanospacing was kept constant, osteogenesis was promoted on the stiff hydrogels, and adipogenesis was favored on the soft

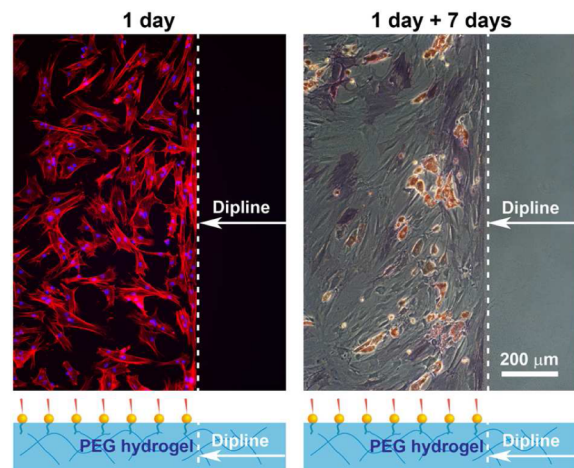


Figure 6. Fluorescence (left) and bright-field (right) micrographs of cells around the diplines on PEG hydrogels. Left: stem cells were cultured in the growth medium for 24 h and immunofluorescently stained to visualize F-actins (red) and nuclei (blue). Right: after 1 day of adhesion, stem cells underwent another 7 days of osteogenic and adipogenic coinduction, followed by ALP and oil-droplet staining. Cells were restricted in the patterned areas even after 8 days of culture and induction, and the background of PEG hydrogels exhibited persistently and potently nonfouling capacity in cell culture medium with 10% serum.

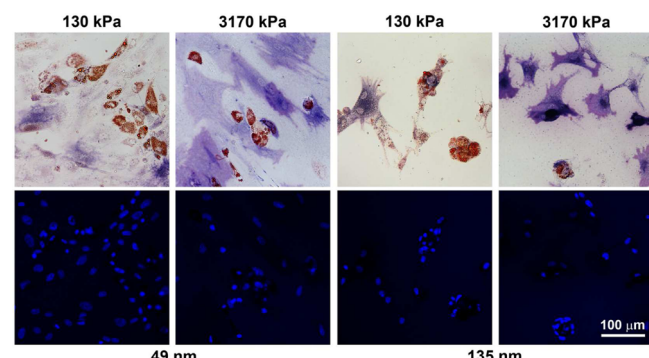


Figure 7. Representative micrographs of cells after osteogenic and adipogenic coinduction. The upper and the lower rows show bright-field images of cells and corresponding fluorescence images of cell nuclei, respectively. ALP positive cells were stained in blue with Fast Blue RR, and oil-droplet positive cells were stained in red with Oil Red O.

hydrogels. Our result was consistent with the observations of stem cell differentiation on unpatterned surfaces.^{25,26} Matrix stiffness did influence lineage specifications of stem cells independently, as surface chemistry difference was eliminated on nanopatterned surfaces at a given RGD nanospacing on the persistently nonfouling PEG hydrogels. When the hydrogel stiffness was controlled, the large RGD nanospacing was beneficial for osteogenesis, while the small RGD nanospacing triggered more adipogenesis due to the competition by osteogenesis in the coinduction, which was in line with our previous study on PEG-700 hydrogels.³⁷

It is known that cell density significantly influences stem cell fate. For instance, denser MSCs prefer adipogenesis rather than osteogenesis, as indicated by Chen group⁵⁶ and Ding group⁴¹ in the examinations of stem cell differentiation on cell culture plates and micropatterned surfaces. However, the density effect cannot be employed to fully interpret the results of stem cell

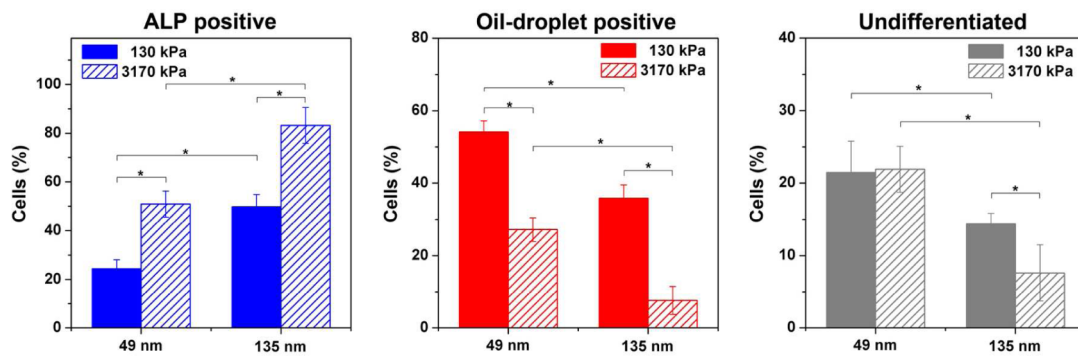


Figure 8. Statistical results of stem cell differentiation as functions of hydrogel stiffness and RGD nanospacing. The percentages of ALP positive cells, oil-droplet positive cells, and undifferentiated cells after coinduction are shown. Mean values and standard deviations from four independent experiments are presented. The stiff hydrogels and/or the large RGD nanospacing favored osteogenesis; the soft hydrogels and/or the small RGD nanospacing favored adipogenesis in such a coinduction experiment. “*”: $p < 0.05$ in a student’s t -test, indicating a significant difference between the two groups.

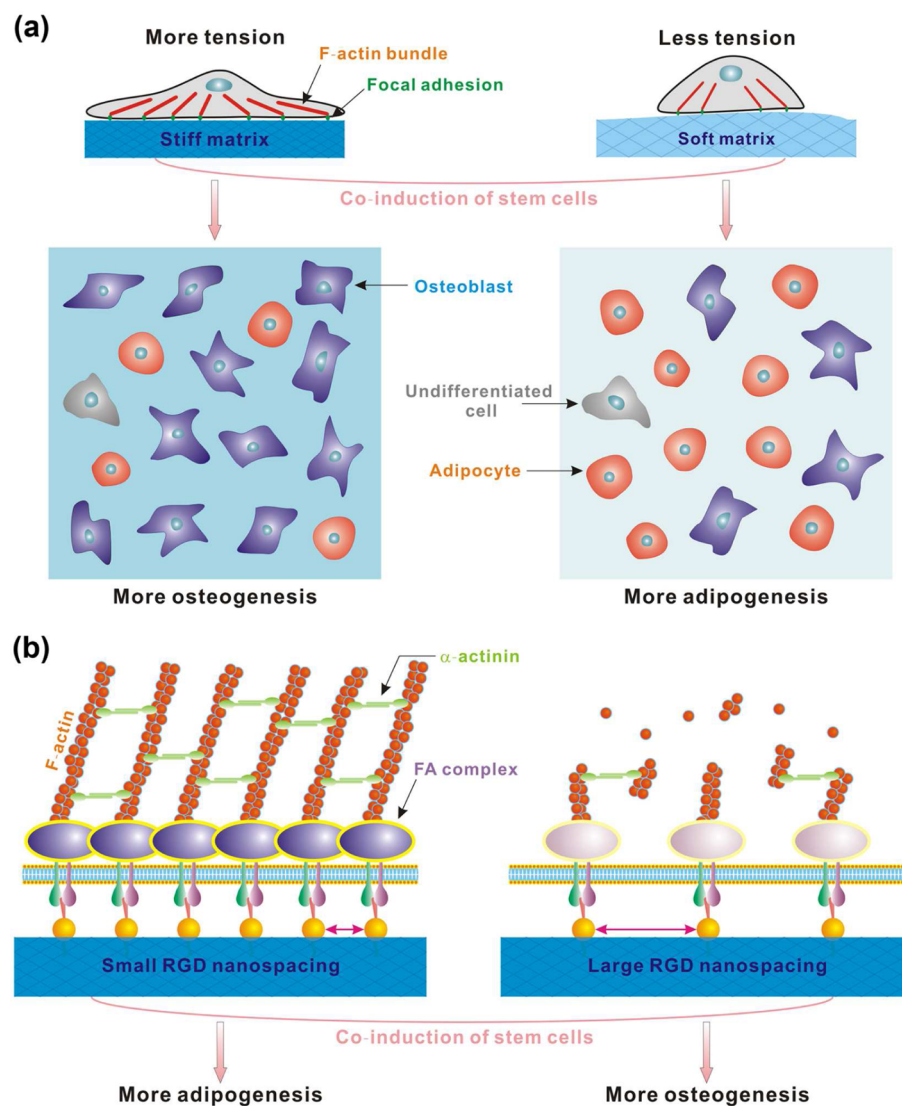


Figure 9. Schematic illustration of the effects of stiffness of matrix and organization of cell-adhesive ligands on stem cells. (a) Matrix stiffness effect. The strong mechanical feedback from a stiff hydrogel leads to more activation of FA complexes and stronger cell tension. The corresponding inside-outside sensing leads to more osteogenesis. (b) RGD nanospacing effect. While focal adhesions are well formed on patterns of a small nanospacing, cells could not form cross-linked actin bundles above the critical adhesion nanospacing (around 70 nm). The large RGD nanospacing favors osteogenesis. The interesting RGD nanospacing effect implies an unknown outside-in signaling pathway.

differentiation on nanopatterned surfaces. Even a contrary trend was observed in some cases. Take the two groups of different matrix stiffnesses under a given small RGD nanospacing (49 nm) as an example. The stiff hydrogels (3170 kPa) exhibited a higher density of adherent MSCs than the relatively softer hydrogels (130 kPa) according to Figure 5b; in contrast, a significantly lower adipogenic differentiation extent was observed in the group of the relatively stiffer hydrogels as reflected by the middle column of Figure 8. On the other hand, the data of varied RGD nanospacings exhibited a consistent trend between cell density and differentiation extents on the surface. For instance, a large RGD nanospacing decreased cell density (Figure 5b) and meanwhile increased the osteogenic fraction (Figure 8, left column). However, the main essential reason for the normal density effect comes from that more cell spreading and thus higher cell tension in the case of lower density enhance osteogenic differentiation of MSCs.^{41,56} On the contrary, the statistical data of spreading areas (Figure 5c) clearly illustrated that cells in the case of the large RGD nanospacing were less spread along with the decrease of the density of adherent cells. Therefore, both matrix stiffness and RGD nanospacing have some unconventional effects on stem cell differentiation, and it is important to decouple matrix stiffness and nanoscale organization of cell-adhesive ligands by using nanotechnology in a deterministic fundamental research.

Our study sheds light on the effect of matrix stiffness on lineage specifications of stem cells, as schematically illustrated in Figure 9a. Cells are capable of sensing and generating internal forces for the measurement of the microenvironment, such as matrix stiffness.^{57,58} When cells are confronted with a stiff hydrogel, cells sense the matrix through integrin-mediated focal adhesions, and more mechanical forces are generated by actin polymerization and myosin II-dependent contractility in order to deform the substrate. FA proteins are able to unfold under mechanical forces and expose binding domains for the downstream proteins or signaling molecules.^{59,60} The strong mechanical feedback from a stiff hydrogel leads to the unfolding of talins, which expose binding domains for vinculins. This further leads to more activation of FA complexes and stronger cell tension, resulting in more osteogenesis. On a compliant hydrogel, the mechanical feedback is not strong enough to activate the formation of FA complexes, and cells generate weaker tension, thus adipogenesis is favored. This regime of mechanotransduction could be referred to as an inside-outside-in sensing, in which cells exert forces on the matrix, and in turn, gauge the mechanical feedback to direct their future destiny. It is important to remind that, although the situation of the large RGD nanospacing is complicated, the effect of hydrogel stiffness on stem cell differentiation still exists, which indicates that matrix stiffness overrides other physical effects in directing stem cell fate.

Our results also demonstrate that RGD nanospacing is an effective modulator of stem cells, no matter on the soft or the stiff hydrogels, as schematically presented in Figure 9b. The small RGD nanospacing triggers the formation of well-organized actin assembly, resulting in stronger cell tension. When the nanospacing is beyond the critical nanospacing of around 70 nm, cells are not capable of forming stable focal adhesions, and actin bundles could not be cross-linked by α -actinin in this case, thus less tension is generated. It is interesting that the large RGD nanospacing promotes osteogenesis although it is not beneficial for specific cell adhesion. Hence, the effect of RGD nanospacing on stem cell

differentiation could not be fully elucidated by cell tension. This might be attributed to an outside-in signaling pathway.

To summarize, we investigate the effects of matrix stiffness and nanoscale spatial organization of cell-adhesive ligands on adhesion and differentiation of stem cells on nanopatterned surfaces. With the nanopatterning techniques, we decouple the stiffness effect from other factors such as protein tethering, and conclude unambiguously that matrix stiffness is an independent and potent regulator of lineage specifications of stem cells. Surface chemistry also regulates stem cell behaviors, as RGD nanospacing affects spreading area and differentiation of rat MSCs. It exhibits an amazing effect on stem cell differentiation via an unknown mechanism. As a consequence, stiffness of matrix and nanoscale organization of cell-adhesive ligands are both vital cues of stem cell microenvironment. The present study affords an in-depth comprehension of cell-ECM interactions, and may be helpful for design of new-generation biomaterials to direct stem cell fate.

■ AUTHOR INFORMATION

Corresponding Author

*E-mail: jdding1@fudan.edu.cn. Tel.: 86 21 65643506. Fax: 86 21 65640293.

Notes

The authors declare no competing financial interest.

■ ACKNOWLEDGMENTS

The authors are grateful for the financial supports from NSF of China (Grant 51273046), Chinese Ministry of Science and Technology (973 program No. 2011CB606203), and Science and Technology Developing Foundation of Shanghai (Grant 13XD1401000).

■ ABBREVIATIONS

PEG, poly(ethylene glycol); RGD, arginine-glycine-aspartate; MSC, mesenchymal stem cell; ECM, extracellular matrix; FA, focal adhesion; PEG-DA, poly(ethylene glycol)-diacrylate; TEA, triethylamine; PBS, phosphate buffer saline; D2959, 2-hydroxy-4'-(2-hydroxyethoxy)-2-methylpropiophenone; PS-*b*-P2VP, poly(styrene-*block*-2-vinylpyridine); TEM, transmission electron microscope; AFM, atomic force microscope; FE-SEM, field-emission scanning electron microscope; DCM, dichloromethane; SD, Sprague-Dawley; DMEM, Dulbecco's modified Eagle medium; FBS, fetal bovine serum; F-actin, filamentous actin; CCD, charge coupled device; ALP, alkaline phosphatase; DAPI, 4',6-diamidino-2-phenylindole

■ REFERENCES

- (1) Discher, D. E.; Mooney, D. J.; Zandstra, P. W. *Science* **2009**, *324* (5935), 1673–1677.
- (2) Watt, F. M.; Huck, W. T. S. *Nat. Rev. Mol. Cell Biol.* **2013**, *14* (8), 467–473.
- (3) Walters, N. J.; Gentleman, E. *Acta Biomater.* **2015**, *11*, 3–16.
- (4) Lutolf, M. P.; Gilbert, P. M.; Blau, H. M. *Nature* **2009**, *462* (7272), 433–441.
- (5) Lee, J.; Abdeen, A. A.; Zhang, D.; Kilian, K. A. *Biomaterials* **2013**, *34* (33), 8140–8148.
- (6) Yao, X.; Peng, R.; Ding, J. D. *Adv. Mater.* **2013**, *25* (37), 5257–5286.
- (7) Murphy, W. L.; McDevitt, T. C.; Engler, A. J. *Nat. Mater.* **2014**, *13* (6), 547–557.
- (8) Dingal, P. C.; Discher, D. E. *Curr. Opin. Biotechnol.* **2014**, *28*, 46–50.

- (9) Mager, M. D.; LaPointe, V.; Stevens, M. M. *Nat. Chem.* **2011**, *3* (8), 582–589.
- (10) Benoit, D. S.; Schwartz, M. P.; Durney, A. R.; Anseth, K. S. *Nat. Mater.* **2008**, *7* (10), 816–823.
- (11) Yao, X.; Hu, Y. W.; Cao, B.; Peng, R.; Ding, J. D. *Biomaterials* **2013**, *34* (36), 9001–9009.
- (12) Kilian, K. A.; Mrksich, M. *Angew. Chem., Int. Ed.* **2012**, *51* (20), 4891–4895.
- (13) Guilak, F.; Cohen, D. M.; Estes, B. T.; Gimble, J. M.; Liedtke, W.; Chen, C. S. *Cell Stem Cell* **2009**, *5* (1), 17–26.
- (14) Discher, D. E.; Janmey, P.; Wang, Y.-L. *Science* **2005**, *310* (5751), 1139–1143.
- (15) Fu, J. P.; Wang, Y. K.; Yang, M. T.; Desai, R. A.; Yu, X. A.; Liu, Z. J.; Chen, C. S. *Nat. Methods* **2010**, *7* (9), 733–736.
- (16) Dalby, M. J.; Gadegaard, N.; Tare, R.; Andar, A.; Riehle, M. O.; Herzyk, P.; Wilkinson, C. D.; Oreffo, R. O. *Nat. Mater.* **2007**, *6* (12), 997–1003.
- (17) Ayala, R.; Zhang, C.; Yang, D.; Hwang, Y.; Aung, A.; Shroff, S.; Arce, F. T.; Lal, R.; Arya, G.; Varghese, S. *Biomaterials* **2011**, *32* (15), 3700–3711.
- (18) Pelham, R. J.; Wang, Y.-L. *Proc. Natl. Acad. Sci. U.S.A.* **1997**, *94* (25), 13661–13665.
- (19) Engler, A.; Bacakova, L.; Newman, C.; Hategan, A.; Griffin, M.; Discher, D. *Biophys. J.* **2004**, *86* (1), 617–628.
- (20) Missirlis, D.; Spatz, J. P. *Biomacromolecules* **2014**, *15* (1), 195–205.
- (21) Lo, C. M.; Wang, H. B.; Dembo, M.; Wang, Y.-L. *Biophys. J.* **2000**, *79* (1), 144–152.
- (22) Tse, J. R.; Engler, A. J. *PLoS One* **2011**, *6* (1), e15978.
- (23) Gilbert, P. M.; Havenstrite, K. L.; Magnusson, K. E.; Sacco, A.; Leonardi, N. A.; Kraft, P.; Nguyen, N. K.; Thrun, S.; Lutolf, M. P.; Blau, H. M. *Science* **2010**, *329* (5995), 1078–1081.
- (24) Rowlands, A. S.; George, P. A.; Cooper-White, J. J. *J. Am. J. Physiol. Cell Physiol.* **2008**, *295* (4), C1037–C1044.
- (25) Engler, A. J.; Sen, S.; Sweeney, H. L.; Discher, D. E. *Cell* **2006**, *126* (4), 677–689.
- (26) Huebsch, N.; Arany, P. R.; Mao, A. S.; Shvartsman, D.; Ali, O. A.; Bencherif, S. A.; Rivera-Feliciano, J.; Mooney, D. J. *Nat. Mater.* **2010**, *9* (6), 518–526.
- (27) Trappmann, B.; Gautrot, J. E.; Connelly, J. T.; Strange, D. G. T.; Li, Y.; Oyen, M. L.; Stuart, M. A. C.; Boehm, H.; Li, B. J.; Vogel, V.; Spatz, J. P.; Watt, F. M.; Huck, W. T. S. *Nat. Mater.* **2012**, *11* (7), 642–649.
- (28) Wen, J. H.; Vincent, L. G.; Fuhrmann, A.; Choi, Y. S.; Hribar, K. C.; Taylor-Weiner, H.; Chen, S. C.; Engler, A. J. *Nat. Mater.* **2014**, *13* (10), 979–987.
- (29) Graeter, S. V.; Huang, J. H.; Perschmann, N.; Lopez-Garcia, M.; Kessler, H.; Ding, J. D.; Spatz, J. P. *Nano Lett.* **2007**, *7* (5), 1413–1418.
- (30) Giancotti, F. G.; Ruoslahti, E. *Science* **1999**, *285* (5430), 1028–1033.
- (31) Dalby, M. J.; Gadegaard, N.; Oreffo, R. O. C. *Nat. Mater.* **2014**, *13* (6), 558–569.
- (32) Xiong, J. P.; Stehle, T.; Zhang, R. G.; Joachimiak, A.; Frech, M.; Goodman, S. L.; Arnaout, M. A. *Science* **2002**, *296* (5565), 151–155.
- (33) Glass, R.; Möller, M.; Spatz, J. P. *Nanotechnology* **2003**, *14* (10), 1153–1160.
- (34) Tran, H.; Killops, K. L.; Campos, L. M. *Soft Matter* **2013**, *9* (29), 6578–6586.
- (35) Cavalcanti-Adam, E. A.; Micoulet, A.; Blummel, J.; Auernheimer, J.; Kessler, H.; Spatz, J. P. *Eur. J. Cell Biol.* **2006**, *85* (3–4), 219–224.
- (36) Arnold, M.; Hirschfeld-Warneken, V. C.; Lohmuller, T.; Heil, P.; Blummel, J.; Cavalcanti-Adam, E. A.; Lopez-Garcia, M.; Walther, P.; Kessler, H.; Geiger, B.; Spatz, J. P. *Nano Lett.* **2008**, *8* (7), 2063–2069.
- (37) Wang, X.; Yan, C.; Ye, K.; He, Y.; Li, Z. H.; Ding, J. D. *Biomaterials* **2013**, *34* (12), 2865–2874.
- (38) Wang, X.; Ye, K.; Li, Z. H.; Yan, C.; Ding, J. D. *Organogenesis* **2013**, *9* (4), 280–286.
- (39) Tang, J.; Peng, R.; Ding, J. D. *Biomaterials* **2010**, *31* (9), 2470–2476.
- (40) Peng, R.; Yao, X.; Ding, J. D. *Biomaterials* **2011**, *32* (32), 8048–8057.
- (41) Peng, R.; Yao, X.; Cao, B.; Tang, J.; Ding, J. D. *Biomaterials* **2012**, *33* (26), 6008–6019.
- (42) Deeg, J. A.; Louban, I.; Aydin, D.; Selhuber-Unkel, C.; Kessler, H.; Spatz, J. P. *Nano Lett.* **2011**, *11* (4), 1469–1476.
- (43) Schvartzman, M.; Palma, M.; Sable, J.; Abramson, J.; Hu, X.; Sheetz, M. P.; Wind, S. J. *Nano Lett.* **2011**, *11* (3), 1306–1312.
- (44) Wang, X.; Li, S. Y.; Yan, C.; Liu, P.; Ding, J. D. *Nano Lett.* **2015**, *15* (3), 1457–1467.
- (45) Arnold, M.; Cavalcanti-Adam, E. A.; Glass, R.; Blummel, J.; Eck, W.; Kantlehner, M.; Kessler, H.; Spatz, J. P. *ChemPhysChem* **2004**, *5* (3), 383–388.
- (46) Huang, J. H.; Graeter, S. V.; Corbellini, F.; Rinck, S.; Bock, E.; Kemkemer, R.; Kessler, H.; Ding, J. D.; Spatz, J. P. *Nano Lett.* **2009**, *9* (3), 1111–1116.
- (47) Yao, X.; Peng, R.; Ding, J. D. *Biomaterials* **2013**, *34* (4), 930–939.
- (48) Aydin, D.; Louban, I.; Perschmann, N.; Blummel, J.; Lohmuller, T.; Cavalcanti-Adam, E. A.; Haas, T. L.; Walczak, H.; Kessler, H.; Fiammengo, R.; Spatz, J. P. *Langmuir* **2010**, *26* (19), 15472–15480.
- (49) Sun, J. G.; Graeter, S. V.; Yu, L.; Duan, S. F.; Spatz, J. P.; Ding, J. D. *Biomacromolecules* **2008**, *9* (10), 2569–2572.
- (50) Kantlehner, M.; Finsinger, D.; Meyer, J.; Schaffner, P.; Jonczyk, A.; Diefenbach, B.; Nies, B.; Kessler, H. *Angew. Chem., Int. Ed.* **1999**, *38* (4), 560–562.
- (51) Huang, J. H.; Ding, J. D. *Soft Matter* **2010**, *6* (15), 3395–3401.
- (52) Perschmann, N.; Hellmann, J. K.; Frischknecht, F.; Spatz, J. P. *Nano Lett.* **2011**, *11* (10), 4468–4474.
- (53) Liu, Y.; Medda, R.; Liu, Z.; Galior, K.; Yehl, K.; Spatz, J. P.; Cavalcanti-Adam, E. A.; Salaita, K. *Nano Lett.* **2014**, *14* (10), 5539–5546.
- (54) Ezzell, R. M.; Goldmann, W. H.; Wang, N.; Parasharama, N.; Ingber, D. E. *Exp. Cell Res.* **1997**, *231* (1), 14–26.
- (55) Platzman, I.; Muth, C. A.; Lee-Thedieck, C.; Pallarola, D.; Atanasova, R.; Louban, I.; Altrock, E.; Spatz, J. P. *RSC Adv.* **2013**, *3* (32), 13293–13303.
- (56) McBeath, R.; Pirone, D. M.; Nelson, C. M.; Bhadriraju, K.; Chen, C. S. *Dev. Cell* **2004**, *6* (4), 483–495.
- (57) Vogel, V.; Sheetz, M. *Nat. Rev. Mol. Cell Biol.* **2006**, *7* (4), 265–275.
- (58) Geiger, B.; Spatz, J. P.; Bershadsky, A. D. *Nat. Rev. Mol. Cell Biol.* **2009**, *10* (1), 21–33.
- (59) Holle, A. W.; Engler, A. J. *Curr. Opin. Biotechnol.* **2011**, *22* (5), 648–654.
- (60) Carisey, A.; Tsang, R.; Greiner, A. M.; Nijenhuis, N.; Heath, N.; Nazgiewicz, A.; Kemkemer, R.; Derby, B.; Spatz, J.; Ballestrem, C. *Curr. Biol.* **2013**, *23* (4), 271–281.